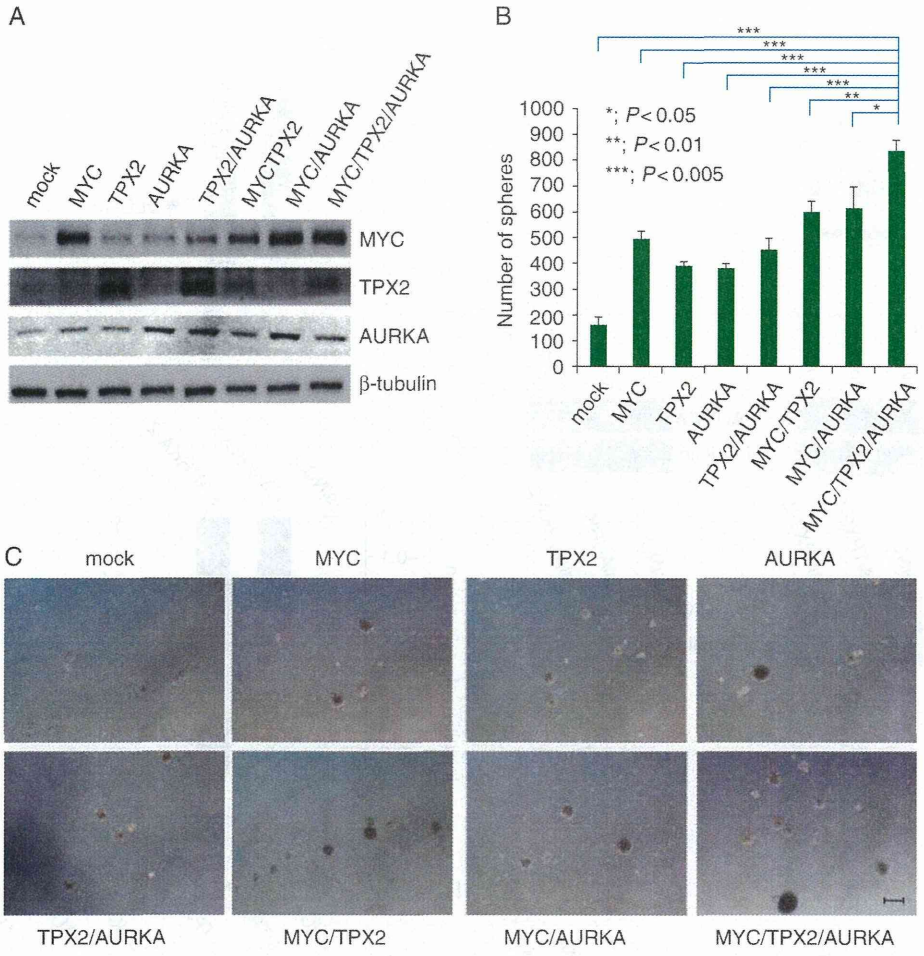

Figure 2. Effects on *MYC*, *AURKA* and *TPX2* on anchorage-dependent growth in normal fibroblast (KMST-6 cells). (A) Indicated combinations of the three genes were ectopically expressed using lentiviral vectors and the expression was confirmed by western blotting. (B) Sphere formation assays with ectopic expression of the three genes. Effects of ectopic expression on anchorage-independent growth are quantified by the number of spheres. Error bars represent the SD from three replicates. (C) Representative images of formed spheres. Scale bar: 100 μm.

although there was no significant difference in *AURKA* knockdown (Figure 3B and C). To analyze the cooperative function of *TPX2* and *AURKA* with *MYC* more clearly, we conducted similar assays in DLD-1 cells stably expressing *MYC* and mock cells (Figure 3D). We found that knockdown of *AURKA* or *TPX2* (Figure 3E) more potently inhibited proliferation of *MYC*-overexpressing DLD-1 cells than that of mock cells (Figure 3F). Collectively, these results suggest the crucial function of the *AURKA/TPX2* axis in maintenance of *MYC*-dependent cancer cells.

AURKA as a therapeutic target in MYC-driven colorectal cancer

Based on the above result, we then tested the possibility of using *AURKA* as therapeutic targets in *MYC*-driven colorectal cancer. Although no *TPX2* inhibitors are currently available, numerous *AURKA* inhibitors have been developed. In this study, we employed the selective *AURKA* inhibitor, MNL8237 (alisertib), which is one of the most potent small-molecule inhibitors of *AURKA* activity [16, 17]. From the result of cell viability assays, we hypothesized that the sensitivity of MLN8237 was dependent on *MYC* expression levels of cancer cells: HCT-116 cells, which highly express *MYC*, were sensitive to MLN8237 at lower concentration than DLD-1 cells, which do not exhibit aberrant *MYC* expression (Figure 4A). We also confirmed this trend by apoptosis assays (Figure 4B). Furthermore, we carried out both the assays using DLD-1 cells ectopically expressing *MYC* and mock cells. Consistently, overexpression of *MYC* increased sensitivity of DLD-1 cells to MLN8237 (Figure 4C and D). These observations were also reproduced in an experiment using a normal fibroblast cell line (KMST-6), where lower concentrations of MLN8237 more effectively suppressed viability of cells with *MYC* ectopic expression than that of unaltered cells (supplementary Figure S5, available at *Annals of Oncology* online). Taken together, our data suggest that *AURKA* could be a therapeutic target for *MYC*-driven cancers.

MYC, AURKA and TPX2 as a poor prognostic indicator

Finally, we analyzed the impact of *MYC*, *AURKA* and *TPX2* expression on the prognosis of colorectal cancer patients. Our qRT-PCR experiments showed that *MYC*, *AURKA* and *TPX2*

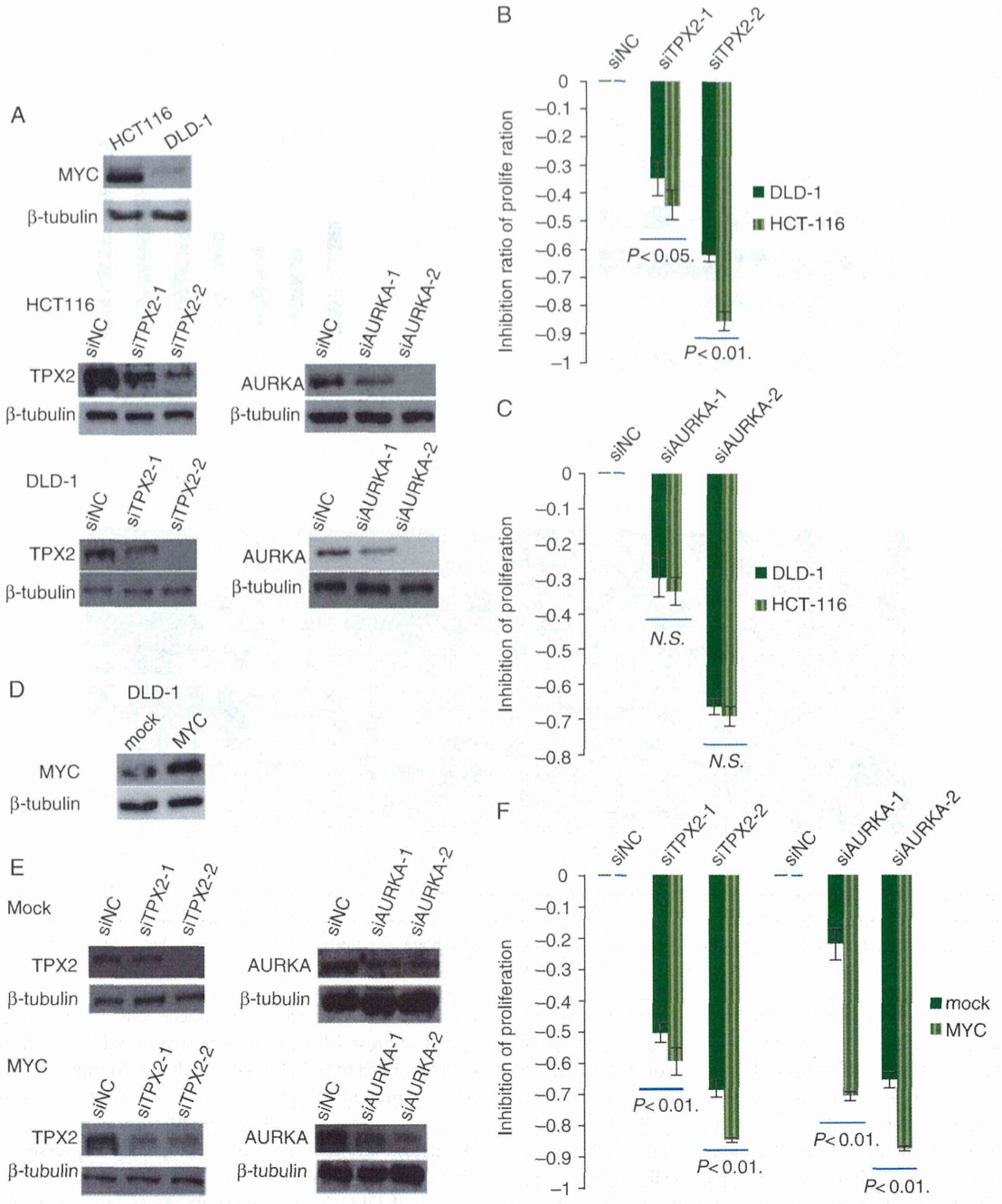

Figure 3. The effects of *AURKA and TPX2* knockdown on proliferation in colorectal cancer cells. (A) Western blotting showing protein levels of *MYC, AURKA* and *TPX2* in HCT-116 cells than in DLD-1 cells. Protein levels of *AURKA* and *TPX2* were measured after transfection of negative control siRNA (siNC) or two different siRNAs for each gene. (B) The inhibition efficiency of cell proliferation of HCT-116 cells and DLD-1 cells by *TPX2* knockdown was analyzed at 72 h after *TPX2* knockdown. *Y*-axis indicates the degree of cell growth inhibition compared with negative control siRNA. Error bars represent the means ± SDs of six independent experiments. (C) The inhibition efficiency of cell proliferation of HCT-116 cells and DLD-1 cells by *TPX2* knockdown was analyzed at 72 h after *AURKA* knockdown. *Y*-axis indicates the degree of cell growth inhibition compared with negative control siRNA. Error bars represent the means ± SDs of six independent experiments. (D) Western blot analyses of mock and *MYC*-expressing DLD-1 cells. (E) TPX2 protein expression after knockdown of *TPX2* and AURKA protein expression after knockdown of *AURKA* by two different siRNAs in mock and *MYC*-expressing DLD-1 cells. siNC, negative control siRNA. (F) The inhibition efficiency of cell proliferation in mock and *MYC*-expressing cells after 72 h of knockdown of *TPX2* and *AURKA*. *Y*-axis indicates the degree of cell growth inhibition compared with negative control siRNA. Error bars represent the means ± SDs of six independent experiments.

expression levels in tumor tissues were significantly higher than those in normal tissues (supplementary Figure S6A, available at *Annals of Oncology* online), and significantly correlated with one another, consistently with frequent co-amplification between 8q24 and 20q (supplementary Figure S6B, available at *Annals of Oncology* online). By combining these expression data with

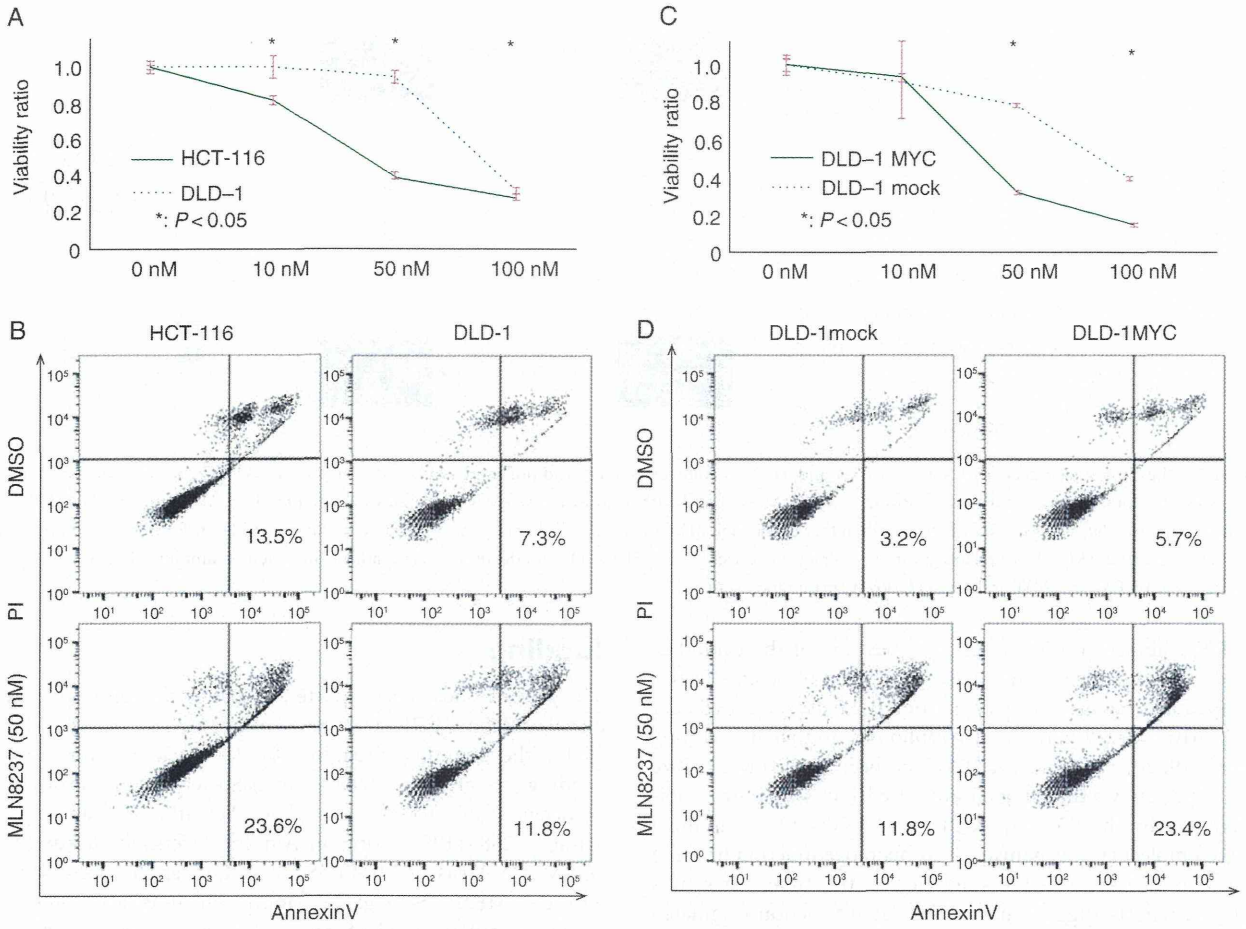

Figure 4. The therapeutic efficacy of an *AURKA*-specific inhibitor, MLN8237 in colorectal cancer cells. (A) The viability of colorectal cancer cell lines treated with MLN8237. MLN8237 was added to the culture medium at a final concentration of 10, 50 or 100 nM for 72 h. Error bars represent the means ± SDs of six independent experiments. (B) Flow cytometry density plots showing control (treated with DMSO; upper panel) and MNL8237-treated (lower panel) colorectal cancer cells (left panel: HCT-116 cells; right panel: DLD-1 cells) stained with AnnexinV-FITC and propidium iodide (PI)-PE. The ratio of apoptotic cells is shown in each panel. (C) The viability of DLD-1 cells treated with MLN8237 was analyzed. MLN8237 was added to the culture medium at a final concentration of 10, 50 or 100 nM for 72 h. Error bars represent the means ± SDs of six independent experiments. (D) Flow cytometry density plots showing control (treated with DMSO; upper panel) and MNL8237-treated (lower panel) DLD-1 cells (left panel: mock; right panel: *MYC*-expressing) stained with AnnexinV-FITC and PI-PE.

survival information, we also confirmed a significant impact of *MYC*, *AURKA* and *TPX2* expression on prognosis of colorectal cancer patients. We divided all 159 cases into three groups, depending on expression levels of the three genes, to find that groups with high expression of *MYC* and *AURKA*/*TPX2* have the poorest overall survival (Figure 5A). To corroborate our findings, we analyzed additional public datasets; we confirmed the expression of *MYC* and *AURKA*/*TPX2* as a prognostic indicator in multiple cancer types, consistently with results from our expression and copy number analyses (supplementary Figure S7, available at *Annals of Oncology* online and Figure 1B). Collectively, our survival analysis also supports the roles of *AURKA* and *TPX2* as driver genes acting cooperatively with *MYC*.

discussion

Through *in silico* analyses and *in vitro* experiments, this study identified *AURKA* and *TPX2* as novel *MYC* co-regulators in colorectal cancer cells. The two interacting genes are located on 20q, which is frequently amplified across many cancer types. Recently, Sillars-Hardebol et al. reported that *AURKA* and *TPX2* on 20q act as driver genes by promoting the progression of colorectal adenoma to carcinoma [18]. Our study added the further insight into the oncogenic functions of the two genes that they act as driver genes cooperatively with *MYC* in *MYC*-driven colorectal tumors. Our copy number data analysis also shows prevailing co-amplification between the *MYC* locus 8q24 and 20q across various types of cancers. Although mechanisms underlying genomic co-amplification have been poorly studied, our data strongly suggest that co-amplification between 8q24 and 20q results from evolutionary selection for the oncogenic interaction between *MYC* and the two 20q driver genes.

A *MYC* co-regulator could be a therapeutic target via a synthetic lethal interaction. In fact, our experiments show an *AURKA* inhibitor is effective for *MYC*-driven colorectal cancer cells. Consistently with our data, several recent studies reported similar synthetic lethal interactions. Kessler et al. conducted genome-wide screen for *MYC* synthetic lethal interaction using

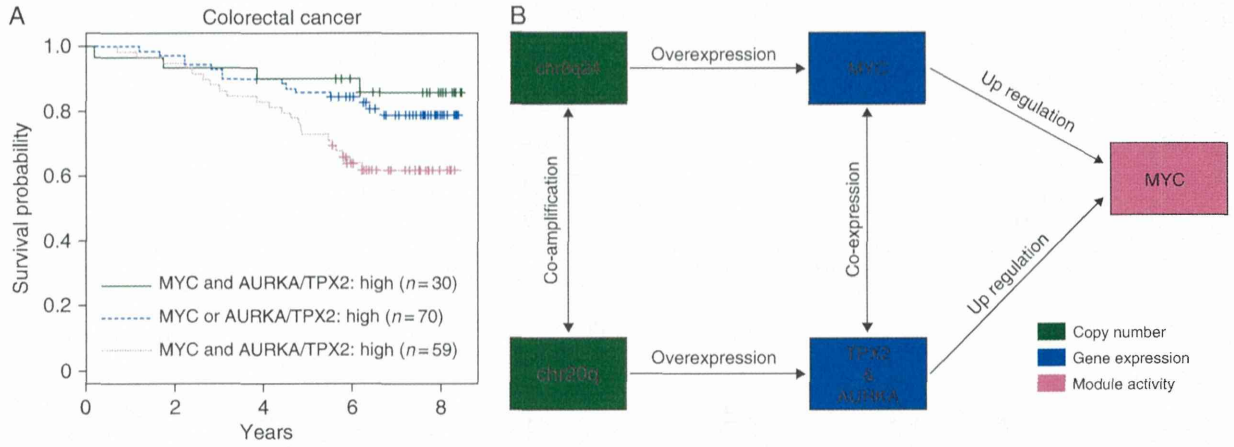

Figure 5. The clinical significance of *MYC*, *AURKA* and *TPX2* in colorectal cancer and our model of the *MYC* pathway. (A) Kaplan–Meier overall survival curves of 159 colorectal cancer patients according to *MYC*, *AURKA* and *TPX2* expression levels. The overall survival of the high *MYC* and *AURKA/TPX2* expression group ($n = 59$) was significantly poorer than that of the high *MYC* or *AURKA/TPX2* expression group ($n = 70$; log-rank test; $P = 0.027$) and that of the low *MYC* and *TPX2/ARUKA* expression group ($n = 30$; log-rank test; $P = 0.025$). (B) Our model of the *MYC* pathway in which co-amplification and co-expression of *AURKA/TPX2* and *MYC* induce *MYC* downstream target genes.

a shRNA library and identified *TPX2* as one of the candidate genes [5]. Targeting aurora kinase has proven to be an effective therapeutic strategy; targeting aurora B kinase (*AURKB*) for *MYC*-driven B-cell and T-cell lymphomas and small cell lung cancer [19, 20]. Moreover, *AURKA* has been proved to stabilize *MYCN* protein via directing a K48 to K63/K11 switch in its ubiquitylation by the E3 ubiquitin ligase *FBXW7* [21]. Although detailed molecular mechanism of co-operative function between *MYC* and *AURKA/TPX2* was not clear at this time, our results and past reports suggest such molecular interaction originated from genomic co-amplification promotes carcinogenesis. Although our experiments were done only for colorectal cancer, high reproducibility in our bioinformatic and survival analyses suggest that the synthetic lethal interaction between *MYC* and the *AURKA/TPX2* axis might be prevailing across diverse types of cancers.

Collectively, this study built a new model of the central network in *MYC*-driven cancer (Figure 5B). Co-amplification between 8q24 and 20q leads to co-overexpression of *MYC* and *AURKA/TPX2*, which cooperatively induce *MYC* downstream target genes. Based on this model, we propose that inhibiting the *AURKA/TPX2* axis would be a novel synthetic lethal therapeutic approach for *MYC*-driven cancers.

acknowledgements

We would like to thank Prof. Okabe (Open Innovation Center for Drug Discovery, University of Tokyo) and Dr Hinohara (Institute of Medical Science, University of Tokyo) for their excellent advice. We also thank to Ms Shimo-oka, Ms Kasagi, Ms Kohno, Ms Oda, Ms Kawano and Ms Aoyagi for their assistance. This research used computational resources of the K computer provided by the RIKEN Advanced Institute for Computational Science through the HPCI System Research project (Project ID: hp140230). Computation time was also provided by the Super Computer System, Human Genome Center, Institute of Medical Science, University of Tokyo.

funding

The present study was supported in part by the following grants and foundation; CREST, Japan Science and Technology Agency (JST), the Funding Program for Next Generation World-Leading Researchers (LS094), Japan Society for the Promotion of Science (JSPS) Grant-in-Aid for Scientific Research, grant number 25861199, Grants-in-Aid for Scientific Research on Innovative Areas of MEXT 'Systems Cancer Research' (4201), and the MEXT Strategic Programs on Innovative Research 'Supercomputational Life Science', and Osaka Cancer Society.

disclosure

The authors have declared no conflicts of interest.

references

1. Kozma L, Kiss I, Szakall S, Ember I. Investigation of c-myc oncogene amplification in colorectal cancer. Cancer Lett 1994; 81: 165–169.
2. Blancato J, Singh B, Liu A, Liao DJ, Dickson RB. Correlation of amplification and overexpression of the c-myc oncogene in high-grade breast cancer: FISH, in situ hybridisation and immunohistochemical analyses. Br J Cancer 2004; 90: 1612–1619.
3. Takahashi Y, Kawate S, Watanabe M et al. Amplification of c-myc and cyclin D1 genes in primary and metastatic carcinomas of the liver. Pathol Int 2007; 57: 437–442.
4. Soucek L, Whitfield J, Martins CP et al. Modelling Myc inhibition as a cancer therapy. Nature 2008; 455: 679–683.
5. Kessler JD, Kahle KT, Sun T et al. A SUMOylation-dependent transcriptional subprogram is required for Myc-driven tumorigenesis. Science 2012; 335: 348–353.
6. Takahashi Y, Sawada G, Kurashige J et al. Paired related homoeobox 1, a new EMT inducer, is involved in metastasis and poor prognosis in colorectal cancer. Br J Cancer 2013; 109: 307–311.
7. Niida A, Smith AD, Imoto S et al. Gene set-based module discovery in the breast cancer transcriptome. BMC Bioinformatics 2009; 10: 71.
8. Niida A, Imoto S, Yamaguchi R et al. Gene set-based module discovery decodes cis-regulatory codes governing diverse gene expression across human multiple tissues. PLoS One 2010; 5: e10910.

9. Bild AH, Yao G, Chang JT et al. Oncogenic pathway signatures in human cancers as a guide to targeted therapies. Nature 2006; 439: 353–357.
10. Popescu NC, Zimonjic DB. Chromosome-mediated alterations of the MYC gene in human cancer. J Cell Mol Med 2002; 6: 151–159.
11. Wood LD, Parsons DW, Jones S et al. The genomic landscapes of human breast and colorectal cancers. Science 2007; 318: 1108–1113.
12. Comprehensive molecular characterization of human colon and rectal cancer. Nature 2012; 487: 330–337.
13. De Luca M, Lavia P, Guarguaglini G. A functional interplay between Aurora-A, Plk1 and TPX2 at spindle poles: Plk1 controls centrosomal localization of Aurora-A and TPX2 spindle association. Cell Cycle 2006; 5: 296–303.
14. Kufer TA, Sillje HH, Korner R et al. Human TPX2 is required for targeting Aurora-A kinase to the spindle. J Cell Biol 2002; 158: 617–623.
15. Barretina J, Caponigro G, Stransky N et al. The Cancer Cell Line Encyclopedia enables predictive modelling of anticancer drug sensitivity. Nature 2012; 483: 603–607.
16. Manfredi MG, Ecsedy JA, Chakravarty A et al. Characterization of Alisertib (MLN8237), an investigational small-molecule inhibitor of aurora A kinase using novel in vivo pharmacodynamic assays. Clin Cancer Res 2011; 17: 7614–7624.
17. Do TV, Xiao F, Bickel LE et al. Aurora kinase A mediates epithelial ovarian cancer cell migration and adhesion. Oncogene 2014; 33: 539–549.
18. Sillars-Hardebol AH, Carvalho B, Tijssen M et al. TPX2 and AURKA promote 20q amplicon-driven colorectal adenoma to carcinoma progression. Gut 2012; 61: 1568–1575.
19. Yang D, Liu H, Goga A et al. Therapeutic potential of a synthetic lethal interaction between the MYC proto-oncogene and inhibition of aurora-B kinase. Proc Natl Acad Sci USA 2010; 107: 13836–13841.
20. Sos ML, Dietlein F, Peifer M et al. A framework for identification of actionable cancer genome dependencies in small cell lung cancer. Proc Natl Acad Sci USA 2012; 109: 17034–17039.
21. Otto T, Horn S, Brockmann M et al. Stabilization of N-Myc is a critical function of Aurora A in human neuroblastoma. Cancer Cell 2009; 15: 67–78.

Carcinogenesis vol.36 no.1 pp.133–141, 2015
doi:10.1093/carcin/bgu232
Advance Access publication November 19, 2014

Epigenetic modulation and repression of miR-200b by cancer-associated fibroblasts contribute to cancer invasion and peritoneal dissemination in gastric cancer

Junji Kurashige[1,2], Kosuke Mima[1,2], Genta Sawada[1,3], Yusuke Takahashi[1,3], Hidetoshi Eguchi[1], Keishi Sugimachi[1], Masaki Mori[3], Kazuyoshi Yanagihara[4], Masakazu Yashiro[5], Kosei Hirakawa[5], Hideo Baba[2] and Koshi Mimori[1,*]

[1]Department of Surgery, Kyushu University Beppu Hospital, 4546 Tsurumihara, Beppu, Oita 874-0838, Japan, [2]Department of Gastroenterological Surgery, Graduate School of Medical Sciences, Kumamoto University, 1-1-1 Honjo, Kumamoto, Kumamoto 860-8556, Japan, [3]Department of Gastroenterological Surgery, Osaka University Graduate School of Medicine, 2-2 Yamada-oka, Suita, Osaka 565-0871, Japan, [4]Division of Translational Research, Exploratory Oncology Research and Clinical Trial Center, National Cancer Center, 6-5-1, Kashiwanoha, Kashiwa, Chiba 277-8577, Japan and [5]Department of Surgical Oncology, Osaka City University Graduate School of Medicine, 1-4-3 Asahi-machi, Abeno-ku, Osaka 545-8585, Japan

*To whom correspondence should be addressed. Tel: +81-977-27-1650; Fax: +81-977-27-1651
Email: kmimori@beppu.kyushu-u.ac.jp

Cancer-associated fibroblasts (CAFs) have recently been linked to the invasion and metastasis of gastric cancer. In addition, the microRNA (miR)-200 family plays a central role in the regulation of the epithelial–mesenchymal transition process during cancer metastasis, and aberrant DNA methylation is one of the key mechanisms underlying regulation of the miR-200 family. In this study, we clarified whether epigenetic changes of miR-200b by CAFs stimulate cancer invasion and peritoneal dissemination in gastric cancer. We evaluated the relationship between miR-200b and CAFs using a coculture model. In addition, we established a peritoneal metastasis mouse model and investigated the expression and methylation status of miR-200b. We also investigated the expression and methylation status of miR-200b and CAFs expression in primary gastric cancer samples. CAFs (CAF-37 and CAF-50) contributed to epigenetic changes of miR-200b, reduced miR-200b expression and promoted tumor invasion and migration in NUGC3 and OCUM-2M cells in coculture. In the model mice, epigenetic changes of miR-200b were observed in the inoculated high-frequency peritoneal dissemination cells. In the 173 gastric cancer samples, the low miR-200b expression group demonstrated a significantly poorer prognosis compared with the high miR-200b expression group and was associated with peritoneal metastasis. In addition, downregulation of miR-200b in cancer cells was significantly correlated with alpha-smooth muscle actin expression. Our data provide evidence that CAFs reduce miR-200b expression and promote tumor invasion through epigenetic changes of miR-200b in gastric cancer. Thus, CAFs might be a therapeutic target for inhibition of gastric cancer.

Introduction

Scirrhous gastric cancer has a very poor prognosis due to its rapid infiltrative invasion and high incidence of peritoneal dissemination (1), and the 5-year survival rate of patients with peritoneal dissemination is only 2% (2). Thus, it is necessary to improve our understanding of the mechanisms involved in the spread of gastric cancer to the peritoneal cavity to identify novel therapeutic targets.

Abbreviations: CAF, cancer-associated fibroblast; EMT, epithelial–mesenchymal transition; FBS, fetal bovine serum; miRNA, microRNA; PBS, phosphate-buffered saline;RT–PCR, reverse transcription–PCR; SMA, smooth muscle actin; TGF, transforming growth factor.

Recent studies have established the importance of the tumor stroma in cancer progression and metastasis (3). Stromal fibroblasts are the major cellular constituents of tumor stroma, and are often referred to as cancer-associated fibroblasts (CAFs). They often display the phenotypes of myofibroblasts, which are characterized by the expression of α-smooth muscle actin (α-SMA) and strong contractility (4). Moreover, CAFs play an important role in the malignant progression of several cancers such as breast, prostate, pancreatic, esophageal and lung cancer, among others, including the initiation, proliferation, invasion and metastasis of cancer cells (5–7). A previous report indicated that gastric fibroblasts play an important role in the progression, growth and spread of scirrhous gastric cancers (8,9).

Recent evidence has emerged that directly or indirectly associates several microRNAs (miRNAs) with the epithelial–mesenchymal transition (EMT), contributing to the now extensive list of EMT-associated transcription factors (10,11). Gregory *et al.* and Park *et al.* demonstrated the clear involvement of the miR-200 family in this process, which consists of five members that can be divided into two clusters: miR-200a/b/429 and miR-200c/141, which map to human chromosomes 1 and 12, respectively (12). The miR-200 family has been suggested to play a central role in the regulation of the EMT process during cancer progression and metastasis. The most prominent gene targets of the miR-200 family are *ZEB1* and *ZEB2*, which are direct repressors of the EMT marker E-cadherin (13). We reported previously that miR-200b was an important regulator of EMT through inhibition of migration and invasion via targeting the mRNAs of *ZEB1* and *ZEB2* in gastric cancer cells (14). Several studies have shown that the miR-200 family inhibits translation of *ZEB1* and *ZEB2* mRNAs in several types of cancers (15–17). Moreover, in addition to the epigenetic regulation of *ZEB1* and *ZEB2* by miR200, previous reports have clarified that aberrant DNA methylation is observed in the promoter region of miR200 family themselves, which occurs subsequent to the induction of EMT by the reactivation of *ZEB1* and *ZEB2* in various cancers (18–20).

In the current study, we demonstrated that the epigenetic mechanisms involved in the regulation of the miR-200 family are not only restricted to malignant cells but are also apparent in CAFs. We found that miR-200b is epigenetically regulated and demonstrated a link between the epigenetics status of miR-200b and the presence of CAFs in gastric cancer cell lines, model mice and cancer tissue samples from patients. The purpose of this study was to evaluate how CAFs are involved in the progression and invasion of the corresponding adjacent cancer cells via epigenetic changes of miR-200b in gastric cancer.

Materials and methods

Cell lines and cell culture

Human gastric cancer cell lines (NUGC3, NUGC4, AGS, MKN1, MKN7, MKN28, MKN45 and AZ521) were obtained in 2012 from the Cell Resource Center for Biomedical Research Institute of Development, Aging and Cancer, Tohoku University, Japan. Human gastric cancer cell lines (OCUM-2M and OCUM-2MD3) and human gastric fibroblast cell lines (CAF-37 and CAF-50) were obtained from gastric carcinoma population maintained at Osaka City University (21,22). The fibroblasts were used in the 3rd through 12th passage in culture and mainly at the 5th passage. To examine the incubating myofibroblast content of orthotopic fibroblasts, immunohistochemical staining was performed as described previously (9). HSC-58 cells were established previously from a patient with scirrhous gastric cancer. HSC-58 cells inoculated into BALB/c nude mice led to dissemination of the tumor cells to the greater omentum, mesenterium, peritoneum and so on and caused ascites in a small number of animals. Cycles of isolation and orthotopic inoculation of the ascitic tumor cells were repeated in the mice for a total of 12 cycles. We obtained two cell lines (58As1Luc and 58As9) that possessed high metastatic potential and showed strong capability of inducing ascites (23). HSC-58, 58As1Luc and 58As9

have no KRAS mutation. NUGC3, NUGC4, AGS, MKN1, MKN7, MKN28, MKN45, AZ521, HSC-58, 58As1Luc and 58As9 cells were cultured in RPMI 1640 with 10% fetal bovine serum (FBS; Life Technologies, Grand Island, NY) with 100 IU/ml penicillin and 100 mg/ml streptomycin. OCUM-2M, OCUM-2MD3, CAF-37 and CAF-50 cells were cultured in Dulbecco's modified Eagle's medium (Nikken, Kyoto, Japan) with the addition of 10% heat-inactivated FBS, 100 IU/ml penicillin, 100 mg/ml streptomycin and 0.5 mM sodium pyruvate. Cells were cocultured in Transwell chambers separated by 8 μm pore filters. Gastric cancer cells (3.0×10^5 cells/700 μl) were placed in the bottom chamber, and CAF-37 and CAF-50 (2.0×10^4 cells/300 μl) were placed in the top chamber. After 5 days, the top chamber was removed, and RNA was isolated from cancer cells. NUGC3, OCUM2M, AZ521, HSC-58, 58As1Luc and 58As9 were authenticated by short tandem repeat–PCR analysis. DNA was extracted by each cell line with QIAamp DNA Mini Kit (QIAGEN) and characterized by short tandem repeat–PCR analysis using GenePrint® 10 System (Promega).

Clinical samples

Primary gastric carcinoma tissue and matched normal gastric epithelium samples were obtained from 173 patients who underwent gastric resection without preoperative treatment at Oita Prefectural Hospital, Kyushu University Beppu Hospital between 1993 and 2003. All tissue samples were immediately cut from gastric resections, placed in RNA Later (Takara, Japan), frozen in liquid nitrogen and stored at −80°C until RNA extraction. Moreover, 53 formalin-fixed, paraffin-embedded gastric cancer tissues from Kyushu University Beppu Hospital were used in this study. Written informed consent was obtained from all patients, and the study protocol was approved by the local ethics committee. Clinicopathological information, including age, gender, pathology, differentiation and tumor-node-metastasis classification, was available for all patients.

Total RNA isolation and first-strand complementary DNA synthesis

Total RNA was isolated from frozen tissue samples by means of the modified acid-guanidine-phenol-chloroform method and isolated from cultured cell lines by using the miRNeasy Mini Kit (QIAGEN), as described previously (24,25). The purity and concentration of all RNA samples were evaluated by the absorbance ratio at 260/280 nm with a NanoDrop ND-1000 spectrophotometer (NanoDrop Technologies, Rockland, DE). Total RNA was reverse transcribed to complementary DNA with M-MLV RT (Invitrogen, Carlsbad, CA).

Quantitative real-time reverse transcription–PCR

The expression of miR-200a, b, miR-429 was determined by TaqMan quantitative real-time reverse transcription–PCR (qRT–PCR) using TaqMan microRNA assay kits (Ambion) according to the manufacturer's protocols, as described previously (14). miR-200a, b, miR-429 expression was normalized to that of the small nuclear RNA *RNU6B*. The expression of *CDH1*, *ZEB1*, *ZEB2* and *Vimentin* was determined using a LightCycler 480 probes master kit (Roche Diagnostics,) according to the manufacturer's instructions. Primers and TaqMan assays are listed in Supplementary Table 1, available at *Carcinogenesis* Online. All qRT–PCRs were run in a LightCycler 480 System II (Roche Diagnostics; USA). The relative amounts of miR-200a, b, miR-429, *CDH1*, *ZEB1*, *ZEB2* and *Vimentin* were measured using the $2^{-\Delta\Delta CT}$ method. All qRT–PCRs were performed in triplicate.

miRNA microarray of HSC-58, 58As1Luc and 58As9

RNA was extracted from each cell line, and RNA samples were dephosphorylated and labeled with Cyanine 3-pCp using T4 RNA ligase by incubating at 16°C for 2 h. After the labeling reaction, the samples were completely dried using a vacuum concentrator at 55°C for 4 h. The dried samples were treated with GE blocking agent. The SurePrint G3 Human v16 miRNA 8×60 K array, which contains probes for 1205 human and 144 human viral miRNAs, was used for miRNA profiling. The blocked samples were hybridized to the probes on the microarray at 55°C with constant rotation at 20 r.p.m. in the Agilent microarray hybridization chamber for 20 h. The microarray slide was washed and scanned using the Agilent scanner to obtain the microarray image. The numerical data for the miRNA profiles were extracted from the image using the Feature Extraction program. These data were analyzed with the aid of GeneSpring GX software, version 7.3 (all from Agilent Technologies). We normalized the observed expression levels of miRNA through the procedure of quantile normalization, and miRNAs displaying an increase or decrease >2-fold were selected for further analysis. MiRNAs that displayed increased and decreased expression are listed in Supplementary Table 2, available at *Carcinogenesis* Online, and Table I, respectively.

DNA methylation analysis and 5-aza-2′-deoxycytidine treatment

CpG islands were identified *in silico* using Methyl Primer Express v1.0 software (Applied Biosystems, Carlsbad, CA). DNA methylation status was established by bisulfite genomic sequencing of multiple clones and methylation-specific PCR. The primer sequences used in the DNA methylation analysis are listed in Supplementary Table 1, available at *Carcinogenesis* Online. Cells were treated with 2.5 or 5.0 μM 5-aza-2′-deoxycytidine (5-aza-dC; Sigma–Aldrich, St Louis, MO) for 48 h.

Table I. Summary of significantly differentially expressed miRNAs in 59As1Luc and 59As9 cells compared with HSC-59 cells

Rank	microRNA	Chromosomal location	Fold change(log2)
Decreased expression in 59As1Luc compared with HSC-58			
1	hsa-miR-31-3p	9p21	−8.42
2	hsa-miR-141-3p	12p13	−8.32
3	hsa-miR-200a-3p	1p36	−5.62
4	hsa-miR-135b-5p	1q32	−5.47
5	hsa-let-7g-5p	3p21	−5.35
6	hsa-miR-98-5p	Xp11	−5.34
7	hsa-miR-532-5p	Xp11	−5.30
8	hsa-miR-27b-3p	9q22	−5.25
9	hsa-miR-10b-5p	2q31	−5.20
10	hsa-let-7d-5p	9q22	−5.19
11	hsa-miR-10a-5p	2q31	−5.06
12	hsa-let-7f-5p	17q21	−4.93
13	hsa-miR-27a-3p	19p13	−4.92
14	hsa-miR-28-5p	3q28	−4.84
15	hsa-miR-23b-3p	9q22	−4.79
16	hsa-miR-192-3p	11q13	−4.74
17	hsa-miR-4284	7q11	−4.67
18	hsa-miR-200b-3p	1p36	−4.45
Decreased expression in 59As9 compared with HSC-58			
1	hsa-miR-141-3p	12p13	−8.84
2	hsa-miR-548ag	4q13	−6.70
3	hsa-miR-4510	15q14	−4.04
4	hsa-miR-520g	19q13	−3.22
5	hsa-miR-130a-3p	11q12	−2.82
6	hsa-miR-520d-3p	19q13	−2.70
7	hsa-miR-338-3p	17q25	−2.67
8	hsa-miR-429	1p36	−2.65
9	hsa-miR-200a-3p	1p36	−2.58
10	hsa-miR-548ai	6q16	−2.45
11	hsa-miR-374a-3p	Xq13	−2.39
12	hsa-miR-520b	19q13	−2.33
13	hsa-miR-135b-5p	1q32	−2.28
14	hsa-miR-200b-3p	1p36	−2.26

Migration and invasion assays

Cell migration and invasion were assessed using the BD Falcon FluoroBlok™ 24 Multiwell Insert System (BD Bioscience, San Jose, CA) using 8 mm pore-sized membranes with Matrigel (for invasion assays) or without Matrigel (for migration assays). In brief, 2×10^4 CAF-37 and CAF-50 cells were placed in 750 μl of medium containing 10% FBS in the lower chamber. The medium containing 10% FBS but no cells were added to the lower chamber of control wells. The NUGC3 cells (1×10^5) were placed in the upper chamber of a 24-well plate with serum-free medium. The cell plate was incubated in a humidified atmosphere (37°C and 5% CO_2). After 48 h incubation, the upper chamber was transferred to a second 24-well plate containing 500 μl/well of 4 μg/ml calcein AM in Hanks' balanced salt solution and incubated for 1 h (37°C and 5% CO_2). Invasive cells that migrated through the membrane were evaluated in a fluorescence plate reader at excitation/emission wavelengths of 485/535 nm. Each independent experiment was performed three times.

Immunohistochemistry and quantitative analysis of α-SMA

Immunohistochemical studies of α-SMA were performed on formalin-fixed, paraffin-embedded surgical sections obtained from patients with gastric cancer. Tissue sections were deparaffinized and boiled in 0.01 mol/l sodium citrate buffer in a microwave for 10 min at 500 W for antigen retrieval. Rabbit anti-α-SMA (ab5694; Abcam, Cambridge, UK), diluted 1:100, was used as the primary antibody. All tissue sections were immunohistochemically stained with the avidin-biotin-peroxidase method (LSAB System HRP; Dako, Kyoto, Japan) and were counterstained with hematoxylin. α-SMA expression in cancer-associated stroma was quantified as the relative percentage of the α-SMA-stained area to the selected field area using an imaging processor, as described previously (26,27). Slides were observed under light microscopy at ×100 magnification, and five regions were selected for every slide at random. The expression was independently evaluated by two of the authors (J.K. and K.M.)

using a blinded protocol design (the observers had no information on clinical outcome or any other clinicopathological data). ImageJ software was used to analyze the positive area percentage and staining intensity in the stroma tissue of every region, and then the average value was calculated from the amount of α-SMA on every slide (Supplementary Figure 1, available at *Carcinogenesis* Online). The muscle layer region was avoided for this assessment because muscle fibers ubiquitously express α-SMA.

Immunoblotting for E-cadherin

For immunoblotting, sodium dodecyl sulfate–polyacrylamide gel electrophoresis of proteins was performed using NuPAGE 4–12% Bis-Tris Gel electrophoresis (Invitrogen), an XCell Sure Lock Mini-cell (Invitrogen), and a Power PAC HC (Bio-Rad). The resolved proteins on the gel were transferred to a nitrocellulose membrane using iBlot Dry Blotting System (Invitrogen). The resulting membranes were blocked with 5% iBlot (Applied Biosystems) and 0.1% Tween-20 (Bio-Rad) in phosphate-buffered saline (PBS) (T-PBS) for 1 h. Membranes were then incubated with primary antibodies. Next, the membranes were washed twice for 5 min in T-PBS, incubated with an horseradish peroxidase-conjugated secondary antibody for 1 h and washed twice for 5 min in T-PBS.

Chemiluminescence detection reagents were incubated with the membranes for 1–5 min, followed by image acquisition using an Image Quant LAS500 (GE Healthcare). Primary antibodies targeted pan actin (NeoMarkers) and a monoclonal antibody against E-cadherin (1:200, BD Bioscience) diluted 1:200.

Orthotropic in vivo *models*

Six-week-old female BALB/c nu/nu mice were purchased from Kyudo Japan and maintained under specific pathogen-free conditions and provided with sterile food, water and cages. Ambient light was controlled to provide regular cycles of 12 h of light and 12 h of darkness. A total of 1×10^6 HSC-58, 58As1Luc and 58As9 cells were inoculated into the gastric wall of each mouse after laparotomy, as described previously (23,28,29). For, assessment of miR-200b influence, a total of 1×10^6 cancer cells [58As9 with Pre-miR™ miRNA Precursor Molecule Negative Control and Pre-miR™ miRNA Precursor Molecule pre-200b (Applied Biosystems, Foster City, CA)] were inoculated into the gastric wall of each mouse. The method of transfection of miRNA was following the past manuscript (14). At 28 days after inoculation, the mice were sacrificed and dissected and peritoneal dissemination, liver metastasis and ascites formation were examined. The number of mesentery nodules >5 mm in diameter was also determined. All animal procedures were performed in compliance with the Guidelines for the Care and Use of Experimental Animals established by the Committee for Animal Experimentation of Kyushu University; these guidelines conform to the ethical standards required by Japanese law and also comply with the guidelines for the use of experimental animals in Japan.

Statistical analysis

All experiments were performed at least three times. Continuous variables are expressed as the means ± standard deviations. The relationship between the expression of miR-200b and the patient clinicopathological characteristics was analyzed using the Student's *t*-test or a chi-square analysis. The overall survival curves were plotted according to the Kaplan–Meier method, and the generalized log-rank test was applied to compare the survival curves. The findings were considered to be significant for *P*-values < 0.05. All tests were performed using JMP software, eighth edition (SAS Institute, Cary, NC).

Results

CAFs stimulated the invasion and migration of gastric cancer via epigenetic change of the miR-200b promoter

We used the coculture system to determine whether CAFs secrete factors that could stimulate the invasion and migration of gastric cancer cells *in vitro*. NUGC3 cells treated with CAFs (CAF-37 and CAF-50) showed significantly high migratory behavior ($P < 0.01$; Figure 1A, left) and were significantly invasive ($P < 0.01$; Figure 1A, right) compared with NUGC3 cells only (NUGC3 control). We examined miR-b expression in the gastric cancer cell lines cocultured with CAFs. The miR-200b expression in NUGC3 and OCUM-2M cells (which showed high miR-200b expression and low methylation) treated with CAFs was lower than those of control cells ($P < 0.05$; Figure 1B). Similarly, the levels of *CDH1* mRNA and protein, an EMT marker, of NUGC3 and OCUM-2M cells treated with CAFs were lower than those of control cells (Figure 1C and E). Recent evidence suggests that expression of miR-200 family members can be epigenetically regulated through methylation of their promoter regions (18,19,30). Therefore, we evaluated the methylation status to identify the mechanism of downregulation of miR-200b by CAFs in gastric cancer. The miR-200b/200a/429 transcription start sites have been determined previously to be located within canonical CpG islands in chromosome 1 (31,32). The CpG islands of the miR-200b promoter in gastric cancer cells treated with CAFs showed an increased amount of partially methylated changes than those of control cell lines (Figure 1D). Moreover, we examined miR-200a and 429 expression in the gastric cancer cell lines cocultured with CAFs. Similarly to miR-200b, the expression of both miR-200a and 429 in NUGC3 cells treated with CAFs were lower than those of control cells (Supplementary Figure 2, available at *Carcinogenesis* Online).

CpG island hypermethylation-associated silencing of miR-200b in cancer cells

miR-200b is suggested to target *ZEB1/2*, thereby preventing the repression of E-cadherin expression by *ZEB1/2*. We evaluated the correlation between miR-200b and *CDH1*, *Vimentin* and *ZEB1/2* mRNA expression in 14 gastric cancer cell lines. As shown in Supplementary Figure 3A–E, available at *Carcinogenesis* Online, the high miR-200b expression cell lines, OCUM-2M, MKN45, KATOIII and OCUM-8, showed low *ZEB1*, *ZEB2* and *Vimentin* expression, whereas the low miR-200b expression cell lines, AZ521 and MKN1, showed high *ZEB1*, *ZEB2* and *Vimentin* expression and low *CDH1* expression. The CpG islands of the miR-200b/200a/429 cluster were almost completely methylated in AZ521 cells, which showed the lowest miR-200b expression, whereas OCUM-2M and NUGC31 cells, which showed high miR-200b expression, were found to be almost completely unmethylated (Supplementary Figure 3F, available at *Carcinogenesis* Online). To further understand the functional significance of promoter hypermethylation of miR-200b, we treated AZ521 cells with the DNA-demethylating agent 5-aza-2′-deoxycytidine. Indeed, treatment of AZ521 with 5-aza-2′-deoxycytidine restored the expression of miR-200b (Supplementary Figure 3G, available at *Carcinogenesis* Online)

The epigenetic change of miR-200b in scirrhous cancer with high peritoneal dissemination

Two highly metastatic cell lines (58As1Luc and 58As9) were also established from the HSC-58 cells. When 58As1Luc or 58As9 cells were implanted orthotopically, bloody ascites began to form ~3 weeks after the inoculation, accompanied by tumor dissemination to the greater omentum, mesenterium, parietal peritoneum, diaphragm and so on, and the mice died soon thereafter (Figure 2A and B). We performed miRNA microarray profiling between HSC-58, 58As1Luc and 58As9 cells. As a result, the miR-200 family was significantly downregulated in 58As1Luc and 58As9 cells compared with HSC-58 cells (Table I). We next performed quantitative RT–PCR to confirm the microarray results. Similarly, miR-200b expression was downregulated in 58As1Luc and 58As9 cells compared with HSC-58 cells (Figure 2C). The CpG islands were partially methylated in 58As1Luc and 58As9 cells, which showed low miR-200b expression; in contrast, CpG islands of HSC-58 cells, which showed high miR-200b expression, were methylated at a much lower frequency (Figure 2D). Treatment with 5-aza-2′-deoxycytidine in 58As1Luc and 58As9 cells restored the expression of miR-200b (Figure 2E). Next, we orthotropically inoculated 58As9 with miR-200b upregulated in the stomach wall of nude mice. After twenty-eight days of orthotropic transplantation, we confirmed miR-200b upregulated markedly were showed that reduction number of disseminated metastasis (Figure 2F).

Association of miR-200b expression with clinicopathological characteristics and survival

Expression of miR-200b was examined in 173 clinical gastric cancer samples using qRT–PCR, with quantified values used to calculate miR-200b/RNU6B ratios. The mean expression of miR-200b

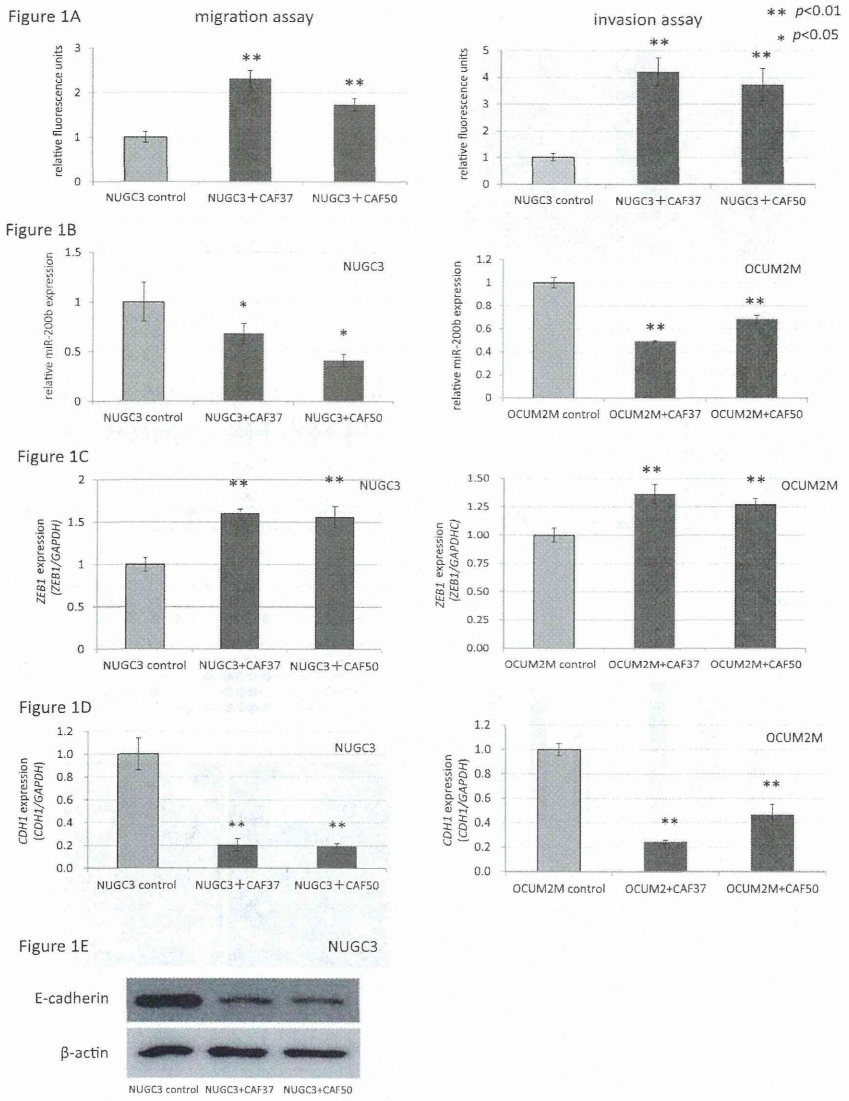

Fig. 1. CAFs stimulated the invasion and migration of gastric cancer via epigenetic changes of the miR-200b promoter. (**A**) NUGC3 cells treated with CAF-37 and CAF-50 showed significantly high migratory and invasive behavior compared with NUGC3 control cells. (**B**) The expression of miR-200b, (**C**) *ZEB1* and (**D**) *CDH1* expression in NUGC3 and OCUM-2M cancer cells in the coculture model. (**E**) The CpG islands of miR-200b in gastric cancer cells showed increased partial methylation in the coculture model. (**F**) E-cadherin expression in NUGC3 and OCUM-2M cancer cells was significantly downregulated in the coculture model.

in cancerous tissue specimens was significantly lower than those in non-cancerous tissues ($P < 0.01$; Figure 3A). Moreover, the mean expression of miR-200b in the cancerous tissue specimens of patients with peritoneal metastasis was significantly lower than those without peritoneal metastasis (peritoneal metastasis included cytology-positive samples; $P < 0.01$; Figure 3B). We divided the 173 gastric cancer patients into two groups according to the median miR-200b expression level: 87 of the cases were placed in the high miR-200b expression group and the remaining 86 cases were placed in the low miR-200b expression group. The association between patient clinicopathological characteristics and miR-200b expression is summarized in Table II. miR-200b expression was significantly associated with cancer differentiation (well and moderately differentiated versus poorly differentiated and others; $P = 0.002$), depth of tumor invasion (T1 and T2 versus T3 and T4; $P = 0.010$), venous invasion (present versus absent; $P = 0.017$), peritoneal metastasis (present versus absent; $P < 0.001$), distant metastasis (including peritoneal metastasis, present versus absent; $P = 0.002$) and cancer staging (stage I and II versus stage III and IV; $P = 0.005$). Analysis of 5-year overall survival showed that the low miR-200b expression group had significantly poorer prognosis than the high expression group ($P = 0.015$; Figure 3C).

Expression of CAFs in gastric cancer stroma and association with miR-200b in gastric cancer specimens

Next, we verified the relationship between the epigenetic status of miR-200b and CAFs surrounding cancer cells in clinical gastric cancer samples. Stromal fibroblasts in 53 gastric cancer samples were quantified using a computer-assisted image analysis system as described in the Materials and methods. A representative photograph stained for α-SMA and the corresponding image treated with an imaging processor are shown in Supplementary Figure 1A–F, available at *Carcinogenesis* Online. The α-SMA staining localized in the cytoplasm of stroma fibroblasts, whereas tumor cells were negatively stained. The α-SMA scores varied from 0.31 to 9.47% (mean, 3.59%). Two investigators (J.K. and K.M.) independently evaluated α-SMA staining and obtained similar results. Next, we examined the correlation between α-SMA staining in gastric cancer stroma

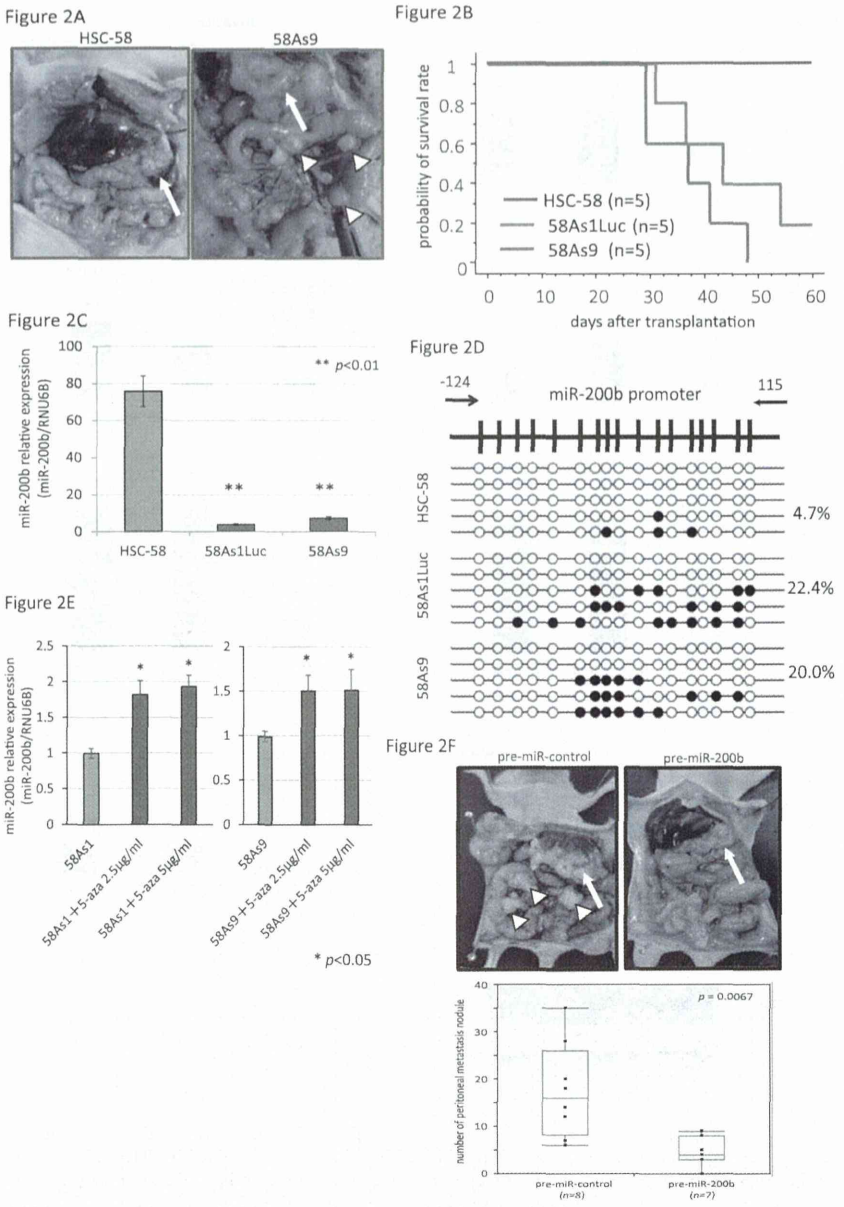

Fig. 2. Silencing miR-200b by epigenetic changes in model mice of scirrhous cancer with high frequency of peritoneal dissemination. (**A** and **B**) 58As9 cells were implanted orthotopically, and bloody ascites began to form ~3 weeks after the inoculation, accompanied by tumor dissemination to the peritoneum; mice with implanted 58As9 cells died faster than mice with implanted HSC-58 cells. White arrows: orthotopic implantation of the cells in the stomach wall of nude mice led to tumor formation within 3 weeks. Blue arrows:, nodules visualized in the abdominal cavity, mesenterium. (**C**) The miR-200b expression in 58As1Luc and 58As9 cells was downregulated compared with HSC-58 cells, as determined by quantitative RT–PCR. (**D**) Whereas HSC-58 cells were found to be unmethylated, the CpG islands of miR-200b promoter regions were partially methylated in 58As1Luc and 58As9 cells. (**E**) Treatment with 5-aza-2′-deoxycytidine in 58As1Luc and 58As9 cells restored the expression of miR-200b. (**F**) Number of disseminated metastasis tumor after 28 days inoculation of 58As9 with miR-200b upregulated. Control, pre-miR-200b are each $n = 8$ and 7.

and miR-200b expression in gastric cancer. There was a significant inverse correlation between miR-200b expression and the α-SMA score (Figure 4A). The gastric cancer samples were then divided into two groups, a high α-SMA group ($n = 26$) and a low α-SMA group ($n = 27$), according to α-SMA expression in stroma at a cut-off point at the median mean value. The patients with high α-SMA expression had significantly lower miR-200b expression than the low α-SMA patients ($P < 0.05$; Figure 4B). When α-SMA expression was compared with the various clinical and pathologic variables listed in Supplementary Table 3, available at *Carcinogenesis* Online, no significant associations were found. Moreover, we chose three low miR-200b/high α-SMA scoring patients and three high miR-200b/low α-SMA scoring patients for further analysis (Supplementary Figure 4, available at *Carcinogenesis* Online). The CpG islands were more significantly methylated in the low miR-200b/high α-SMA group than in the high miR-200b/low α-SMA group (Figure 4C).

Discussion

In this study, we demonstrated that CAFs reduced miR-200b expression and induced the hypermethylation of the miR-200b promoter regions. Furthermore, there was a negative correlation between miR-200b expression in gastric cancer specimens and α-SMA